Entropy **2014**, *16*, 1808-1818; doi:10.3390/e16031808

OPEN ACCESS

entropy

ISSN 1099-4300

www.mdpi.com/journal/entropy

Article

Entropy Change during Martensitic Transformation in $Ni_{50-x}Co_xMn_{50-y}Al_y$ Metamagnetic Shape Memory Alloys

Xiao Xu [1,*], Wataru Ito [2], Takeshi Kanomata [1,3] and Ryosuke Kainuma [1]

[1] Department of Materials Science, Graduate School of Engineering, Tohoku University, Sendai 980-8579, Japan; E-Mail: kainuma@material.tohoku.ac.jp (R.K.)

[2] Department of Materials and Environmental Engineering, Sendai National College of Technology, Natori 981-1239, Japan; E-Mail: ito@sendai-nct.ac.jp (W.I.)

[3] Research Institute for Engineering and Technology, Tohoku Gakuin University, Tagajo 985-8537, Japan; E-Mail: kanomata@tjcc.tohoku-gakuin.ac.jp (T.K.)

* Author to whom correspondence should be addressed; E-Mail: xu@material.tohoku.ac.jp (X.X.); Tel.: +81-22-795-5256; Fax: +81-22-795-5256.

Received: 12 February 2014; in revised form: 18 March 2014 / Accepted: 19 March 2014 / Published: 24 March 2014

Abstract: Specific heat was systematically measured by the heat flow method in $Ni_{50-x}Co_xMn_{50-y}Al_y$ metamagnetic shape memory alloys near the martensitic transformation temperatures. Martensitic transformation and ferromagnetic–paramagnetic transition for the parent phase were directly observed via the specific heat measurements. On the basis of the experimental results, the entropy change was estimated and it was found to show an abrupt decrease below the Curie temperature. The results were found to be consistent with those of earlier studies on Ni-Co-Mn-Al alloys.

Keywords: entropy change; specific heat; thermal transformation arrest; kinetic arrest; metamagnetic shape memory alloy; martensitic transformation; Ni-Co-Mn-Al

1. Introduction

Since the discovery of magnetostructural transition [1] and the metamagnetic shape memory effect [2] in NiMn-based Heusler alloys, numerous research studies have been performed since the alloys are hopeful candidates for application as magnetic actuators [3] and magnetocaloric refrigerants [4]. Currently developed metamagnetic shape memory alloys include Ni-(Co)-Mn-In [2,5], Ni-Co-Mn-Sn

[6], Ni-Co-Mn-Ga [7] and Ni-Co-Mn-Al [8] systems. Among these alloy systems, because of the low cost, several groups have also focused on the Ni-Co-Mn-Al system. To develop magnetocaloric materials, attempts have been made to evaluate isothermal entropy change [9] as well as adiabatic temperature change [10]. Other groups have also investigated the properties of sputtered film [11] and melt-spun ribbon samples [12].

In addition to the application aspect, the Ni-Co-Mn-Al alloys also show interesting fundamental physical phenomena similar to those of other NiMn-based alloys. Like Ni-(Co)-Mn-In alloys [13,14], the thermal transformation arrest (TTA) phenomenon has been observed for $Ni_{45}Co_5Mn_{31}Al_{19}$ (Co_5Al_{19}; we adopt the denotation of $Ni_{50-x}Co_xMn_{50-y}Al_y$ as Co_xAl_y in this article) [15] and $Co_{10}Al_{17}$ [16] alloys. The temperature dependence of entropy change during martensitic transformation shows an abrupt decrease above the TTA temperature and becomes almost zero below it [15]. On the other hand, the kinetic behaviors, enlargement of magnetic-field hysteresis has also been observed for Co_5Al_{19} [15] and $Co_{10}Al_{17}$ [16], as has also been observed for Ni-(Co)-Mn-In [5,14] alloys. For Ni-Co-Mn-Sb and Ni-Co-Mn-In alloys, the temperature hysteresis during martensitic transformation [17] as well as the magnetic field hysteresis [18,19] during magnetic field-induced transition obviously vary with different sweeping rates of temperature and magnetic field. For Co_5Al_{19}, however, an almost equivalent hysteresis has been found by comparison between the results under a pulsed magnetic field and a steady magnetic field [15].

For both the application and fundamental aspects, the entropy change during martensitic transformation is of great importance. Some systematic work has been performed on Ni-Mn-In-X alloys [5,14,20–23], Ni-Mn-Sn-X alloys [22,24] and Ni-Mn-Ga-X alloys [25,26]. However, for the Ni-Co-Mn-Al system, there are currently only indirect calculations for a single alloy [15] and estimations deduced from the Maxwell equation [9]. Very recently, we reported the pseudo-binary magnetic phase diagram of the Co_xAl_y alloys [16]. This phase diagram is shown in Figure 1, where the Al content dependence of martensitic transformation starting temperature T_{M_s} and the Curie temperature of the parent phase T_{C_P} are shown. Based on these alloys reported in the phase diagram, a systematical investigation on the transformation entropy change ΔS for Co_xAl_y alloys by direct measurement was performed.

Figure 1. The magnetic phase diagram for $Ni_{50-x}Co_xMn_{50-y}Al_y$ (Co_xAl_y) alloys reported by X. Xu *et al.* [16] is shown. The martensitic transformation starting temperature T_{M_s} and the Curie temperature of the parent phase T_{C_P} are shown. T_{M_s} and T_{C_P} reported by R. Kainuma *et al.* [27], A. Okubo *et al.* [28] and Y. Kim *et al.* [9] are also plotted. T_A represents for the thermal transformation arrest (TTA) temperature.

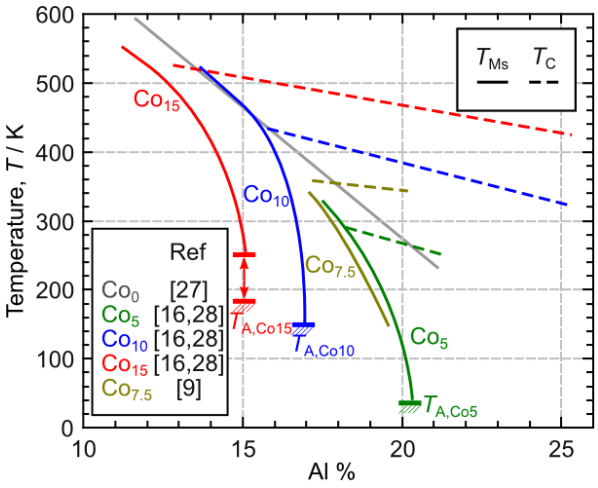

2. Experimental Methods

Refer to Ref. [16] for details of the preparation of the Co_xAl_y samples. Specific heat from around 150 up to 663 K was measured by the heat flow method using a commercial Netzsch DSC 204 F1 Phoenix® equipped with a μ sensor, the measurements being calibrated using a standard sapphire sample according to DIN 51007. Some of the samples, which are listed in Table 1 in Ref. [16], were subjected to composition measurements by EPMA. Since their compositions were very close to the nominal compositions, the nominal compositions were directly used in this research for simplicity.

Figure 2. For $Ni_{50-x}Co_xMn_{50-y}Al_y$ (Co_xAl_y) alloys without martensitic transformation behavior, only the Curie temperatures of the parent phase are observed during the specific heat measurements and are indicated by T_{C_P}. The values of T_{C_P} are taken from Ref. [16].

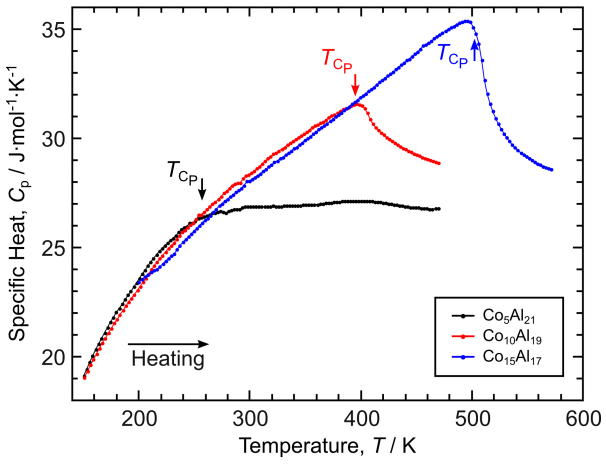

3. Experimental Results

Figure 2 shows the specific heat measurements for Co_xAl_y alloys without martensitic transformation. A strong bending of the baseline was observed for Co_5Al_{21} while typical lambda-shaped peaks were observed for $Co_{10}Al_{19}$ and $Co_{15}Al_{17}$. According to our previous report [16], these peaks correspond to the Curie temperature of the parent phase. The Curie temperatures, indicated by T_{C_P} in the figure, are taken from Ref. [16]. It can be seen that, with increasing Co content, not only the value of T_{C_P}, but also the specific heat around the T_{C_P} increases. It has been reported that for the Co_xAl_{25} alloys, the magnetic moment increases with increasing Co content [28]. Therefore, a higher Co content results in a larger lambda-shaped peak of the specific heat around T_{C_P}, which is contributed to by the strong spin fluctuation [29] near and above the T_{C_P}.

Figure 3. For $Ni_{50-x}Co_xMn_{50-y}Al_y$ (Co_xAl_y) alloys, the results of specific heat obtained by DSC measurements are shown. Peak temperature T_P of the heating process for the martensitic transformation is determined for each sample. Transformation enthalpy change ΔH and the Curie temperature of the parent phase T_{C_P} are also indicated. Since the T_{C_P} slightly varies with different Al content, the T_{C_P} in the figures is shown as a temperature range.

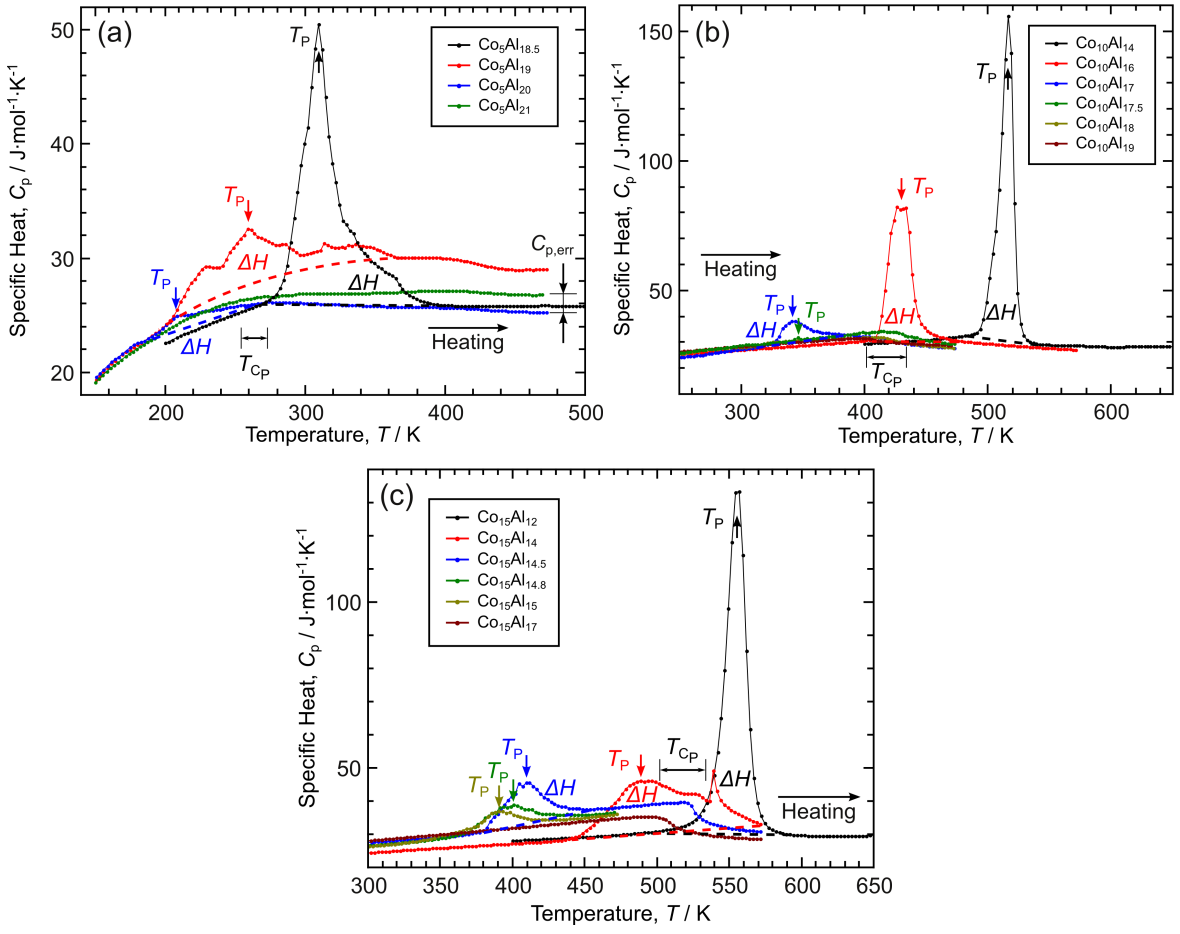

Figure 3(a) shows the specific heat curves for Co_5Al_y alloys. Only the heating process was measured, in order to avoid the complexity of $B2 \rightarrow L2_1$ diffusion which occurs at relatively high temperatures.

For $Co_5Al_{18.5}$ to Co_5Al_{20}, first-order transformations, which correspond to the reverse martensitic transformation, were detected. Reverse martensitic transformation temperature is defined as the peak temperature shown as T_P since this is the temperature with the largest heat absorption. Transformation enthalpy change ΔH was obtained by calculating the area of the peaks, as shown by the dashed lines in the figure. Generally, straight lines connecting both the baselines were used to determine the area. For Co_5Al_{19}, however, since the baseline obviously bends around T_P and the transformation interval, *i.e.*, the difference between the starting and finishing temperatures is very large, a cubic polynomial fitting rather than a linear one was used to determine the baseline. Hence the transformation entropy change ΔS can be calculated by

$$\Delta S = \frac{\Delta H}{T_P}. \quad (1)$$

The obtained T_P, ΔH and ΔS are listed in Table 1. For Co_5Al_{20}, since the TTA phenomenon has been reported even under zero magnetic field [15], it was impossible to obtain a full martensitic transformation during the current DSC measurement. Thus, its ΔH and ΔS are shown with parentheses in Table 1, indicating an underestimation. It can be seen that the ΔH drastically decreases with decreasing T_P. Here, note that for the specific heat data shown in Figure 3, at temperatures away from the martensitic transformation, the values show the specific heat of the sample, whereas for the temperature range near the martensitic transformation, the amount of latent heat is added due to the nature of the heat flow method. According to DIN 51007, the absolute values of the specific heat were calculated based on the assumption that the system backgrounds during each measurement are identical. However, a small change of the system background may exist and this may correspond to a small amount of error of several $J \cdot mol^{-1}K^{-1}$, shown as $C_{p,err}$ in Figure 3(a). (Also note that Figure 3(a) is an enlarged view compared to the scales in Figures 3(b) and 3(c)) However, the error $C_{p,err}$ hardly affects on the determination of ΔS. As shown in Figure 3(a), bending of the baseline instead of the typical lambda-shaped peak was observed for Co_5Al_{20} and Co_5Al_{21} at the T_{C_P}. The reported T_{C_P}s [16] are indicated in the figure.

Figure 3(b) shows the specific heat curves for $Co_{10}Al_y$. Results similar to those in Figure 3(a) were obtained. However, for $Co_{10}Al_y$, magnetic transition of the parent phase was clearly observed, which is indicated in the figure. For $Co_{10}Al_{17.5}$, ΔH and ΔS were likely underestimated due to the TTA phenomenon [16].

For $Co_{15}Al_y$, Figure 3(c) shows the results of specific heat measurements. For the series of $Co_{15}Al_y$, the samples have very close compositions; therefore, it is quite apparent that the ΔH gradually decreases with decreasing T_P.

Table 1. Transformation peak temperature (T_{P}), enthalpy change (ΔH) and entropy change (ΔS) determined by DSC are listed for the reverse martensitic transformations of $Ni_{50-x}Co_xMn_{50-y}Al_y$ (Co_xAl_y). ΔH was calculated from the area shown in Figure 3. Numbers with parentheses suggest possible underestimations. Here the unit of molar mass is taken to be molar atoms, rather than molar molecules.

Nominal	T_{P} /K	ΔH /kJ · mol^{-1}	ΔS /J · mol^{-1}K^{-1}
$Co_5Al_{18.5}$	309.7	0.764	2.47
Co_5Al_{19}	260.0	0.362	1.39
Co_5Al_{20}	212.8	(0.103)	(0.482)
Co_5Al_{21}	-	-	-
$Co_{10}Al_{14}$	517.0	1.71	3.31
$Co_{10}Al_{16}$	430.2	1.18	2.73
$Co_{10}Al_{17}$	341.6	0.295	0.864
$Co_{10}Al_{17.5}$	344.8	(0.0835)	(0.242)
$Co_{10}Al_{18}$	-	-	-
$Co_{10}Al_{19}$	-	-	-
$Co_{15}Al_{12}$	555.9	1.85	3.32
$Co_{15}Al_{14}$	487.2	1.20	2.46
$Co_{15}Al_{14.5}$	410.9	0.419	1.02
$Co_{15}Al_{14.8}$	401.4	0.282	0.703
$Co_{15}Al_{15}$	390.8	0.196	0.501
$Co_{15}Al_{17}$	-	-	-

4. Discussion

The data of ΔS shown in Table 1 are plotted against the Al content in Figure 4(a), together with the $T_{\mathrm{C_P}}$ reported for the Co_xAl_y alloys [16]. The same tendency for ΔS to decrease with increasing Al content was also found in all the series. It is important to note that the transformation type changes at $T_{\mathrm{C_P}}$, *i.e.*, a paramagnetic parent to paramagnetic martensite transformation is to the left side of $T_{\mathrm{C_P}}$ while a ferromagnetic parent to paramagnetic martensite transformation is to the right side of $T_{\mathrm{C_P}}$. Hence, on crossing the $T_{\mathrm{C_P}}$, it was found that the ΔS begins to abruptly decrease, which shows similar behavior to that of Ni-Co-Mn-In alloys [22,23,30]. It is of great importance that this behavior of ΔS may be one of the vital evidences showing the influence of magnetism on the phase stability as well as the magnetostructural transformations. As shown in Figure 2, the magnetic contribution to entropy changes with the Curie temperature, therefore the ferromagnetic ordering should also influences greatly on the stability of the parent phase. This is consistent with the earlier reported experimental results as well as theoretical predictions [22,31]. Moreover, the magnetic contribution may also affect the modes of lattice

vibration, and an stabilization effect of the parent phase may also exist, as the impact on the martensite phase in Ni-Mn-Ga [32,33]. A systematical study and selective comparison between representative metamagnetic and ferromagnetic shape memory alloys are required to further understand this question.

In Figure 4(b), the ΔS is plotted against T_{P}, and the earlier data for Co_5Al_{19} [15] and $Co_{10}Al_{17}$ [16] are also plotted. It can be seen that ΔS decreases with decreasing T_{P} and approaches zero at an efficiently low temperature. A general consistency was found.

Figure 4. Martensitic transformation entropy change ΔS for $Ni_{50-x}Co_xMn_{50-y}Al_y$ (Co_xAl_y) alloys shown in Table 1 is plotted against (a) Al content and (b) transformation peak temperature T_{P}. ΔS reported for Co_5Al_{19} [15] and $Co_{10}Al_{17}$ [16] are also plotted against the measurement temperature in (b). $T_{\mathrm{C_P}}$ means the Curie temperature of parent phase and T_{A} indicates the thermal transformation arrest (TTA) temperature. Both the solid and dashed lines in (a) and (b) are guides for the eye.

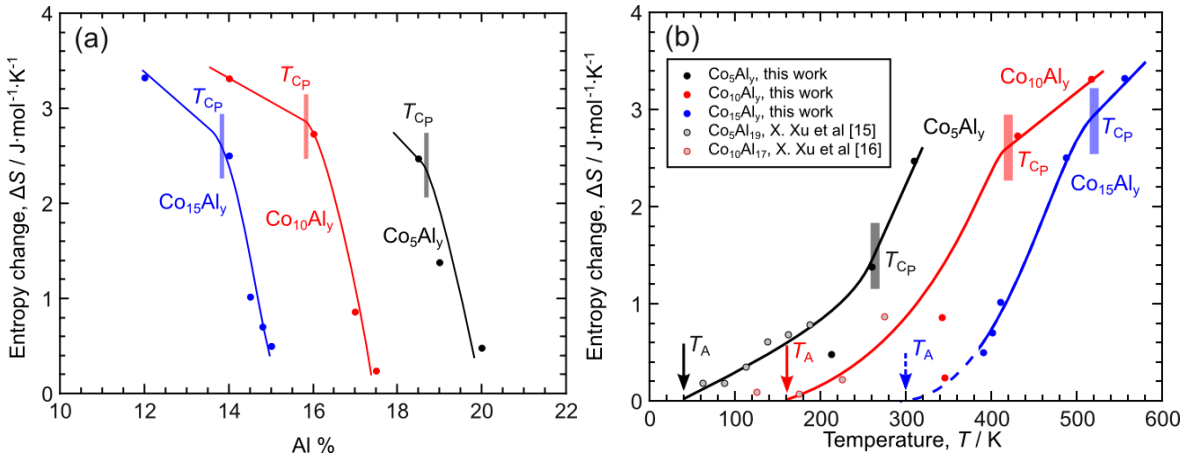

ΔS for Co_7Al_y film was also estimated using the data reported by S. Rios *et al.* [11]. Using the Clausius-Clapeyron equation

$$\Delta S = -\Delta M \cdot \frac{\mathrm{d}H}{\mathrm{d}T}, \tag{2}$$

where $\mathrm{d}T/\mathrm{d}H = 2.1$ K/T [11] is the martensitic transformation shift under different magnetic fields. $\Delta M \approx 585$ emu/cc is the magnetization difference between parent and martensite phases estimated from Figure 3(a) in Ref. [11], where the magnetization for the martensite phase is taken to be zero. Taking the lattice parameter to be $a = 2.88$ Å [11,28], the ΔS is calculated to be 4.0 J/mol·K at 173 K (not plotted in Figure 4(b)). This value is much larger than those of other reports shown in Figure 4(b). The possibility of overestimation here can be considered as follows. First, when calculating the ΔM, the magnetization for the martensite phase was taken to be zero. However, this may not be true since the sample by S. Rios *et al.* had been subjected to ageing heat treatment [11]. Though systematical research for the magnetic properties of the aged martensite phase in Ni-Co-Mn-Al alloys has not been performed to date, with reference to similar alloy systems such as Ni-Mn-In [34], Ni-Co-Mn-Ga [35], and Ni-Mn-Ga [36], there is a possibility of an increase in magnetization in the martensite phase. Note that as long as the heat treatment is kept as the condition in this research, *i.e.*, no ageing treatment at low temperature being performed, the martensite phase has a paramagnetic-like weak magnetism, as reported

for Co_5Al_y and $Co_{10}Al_y$ [8]. Thus, an overestimated ΔM may have resulted in the overestimation of ΔS. Second, the Co_7Al_y film undergoes a martensitic transformation with large thermal hysteresis where the TTA phenomenon occurs. Therefore, the actual value of $\mathrm{d}T/\mathrm{d}H$ might be much larger than 2.1 K/T. Actually, the $\mathrm{d}T/\mathrm{d}H$ approaches infinity at the TTA temperature, and a $\mathrm{d}T/\mathrm{d}H$ as large as 100 K/T can be estimated from Figure 3(b) in Ref. [16].

Moreover, for the Co_xAl_y alloys shown in Figure 4(b), the temperature at which ΔS becomes zero should correspond to the TTA temperature T_A. The T_As are indicated for Co_5Al_y, $Co_{10}Al_y$ and $Co_{15}Al_y$. The values of T_As for Co_5Al_y (40 K) and $Co_{10}Al_y$ (160 K) show good consistency with earlier reports [15,16]. For $Co_{15}Al_y$, the interval of the martensitic transformation is very large and MFIT measurement for it has not been successfully performed even with pulsed magnetic fields up to 55 T. Therefore, we do not have any information on ΔS at low temperature for this series. The dashed line in Figure 4(b) roughly extrapolates the T_A for $Co_{15}Al_y$, assuming that the temperature dependence of ΔS has a shape similar to those of Co_5Al_y and $Co_{10}Al_y$. This gives a value of about 300 K, which is much higher than 190 K, which is reported from thermomagnetization measurements [16]. The reason is discussed as follows. First, as shown in Figure 3(c), the Al content dependence of T_P is very large, and the composition measurements by EPMA also found that the composition difference between different grains is as large as several permillage. This may result in an obvious transformation temperature distribution inside the sample, resulting in an underestimation of T_A by thermomagnetization measurements. Second, as shown in Figure 1, the $T_{\mathrm{C_P}}$ decreases with increasing Al content when the Co content is held constant. Generally the ΔS begins to decrease abruptly only below the $T_{\mathrm{C_P}}$ [22,37]; therefore, a higher T_A can be observed in a sample with a higher $T_{\mathrm{C_P}}$. Hence, a T_A distribution may exist in the sample if the sample has Co or Al inhomogeneity. Third, the Ni-Co-Mn-Al alloy system shows much better ductility than other NiMn-based alloy systems, where even polycrystalline samples can be subjected to compression testing and show superelasticity behavior [38]. Hence, a strong binding in the grain boundary can be expected, and the constraint by the grain boundary may become nucleation sites for the martensitic transformation. Thus, martensitic transformation may still occur at the grain boundary due to this non-chemical reason at a temperature at which martensitic transformation otherwise would have stopped. This reason can also result in an underestimation of the T_A by thermomagnetization measurements. However, in order to measure the T_A for $Co_{15}Al_y$ precisely, use of a stronger non-destructive pulsed magnet [39] is necessary. Nevertheless, a rough estimation of the T_A as 190–300 K can still be concluded based on the results of the present study.

5. Conclusions

In this research, specific heat measurements by the heat flow method were performed systematically on $Ni_{50-x}Co_xMn_{50-y}Al_y$ metamagnetic shape memory alloys. Second-order ferromagnetic–paramagnetic transition as well as first-order martensitic transformation were directly observed via specific heat measurements. The transformation entropy change ΔS was estimated from the latent heat by the specific heat measurements. The ΔS decreases with increasing Al content under the series with fixed Co content. The decreasing tendency enlarges below the Curie temperature of the parent phase. The ΔS estimated in this work was found to be consistent with findings of earlier reports.

Acknowledgements

This work was supported by a Grant-in-Aid for Scientific Research and by a grant from the Japan Society for the Promotion of Science (JSPS).

Conflict of Interest

The authors declare no conflict of interest.

References

1. Sutou, Y.; Imano, Y.; Koeda, N.; Omori, T.; Kainuma, R.; Ishida, K.; Oikawa, K. Magnetic and martensitic transformations of NiMnX(X = In,Sn,Sb) ferromagnetic shape memory alloys. *Appl. Phys. Lett.* **2004**, *85*, 4358–4360.
2. Kainuma, R.; Imano, Y.; Ito, W.; Sutou, Y.; Morito, H.; Okamoto, S.; Kitakami, O.; Oikawa, K.; Fujita, A.; Kanomata, T.; Ishida, K. Magnetic-field-induced shape recovery by reverse phase transformation. *Nature* **2006**, *439*, 957–960.
3. Karaca, H.E.; Karaman, I.; Basaran, B.; Ren, Y.; Chumlyakov, Y.I.; Maier, H.J. Magnetic field-induced phase transformation in NiMnColn magnetic shape-memory alloys-A new actuation mechanism with large work output. *Adv. Funct. Mater.* **2009**, *19*, 983–998.
4. Krenke, T.; Duman, E.; Acet, M.; Wassermann, E.; Moya, X.; Manosa, L.; Planes, A. Inverse magnetocaloric effect in ferromagnetic Ni-Mn-Sn alloys. *Nat. Mater.* **2005**, *4*, 450–454.
5. Umetsu, R.Y.; Ito, W.; Ito, K.; Koyama, K.; Fujita, A.; Oikawa, K.; Kanomata, T.; Kainuma, R.; Ishida, K. Anomaly in entropy change between parent and martensite phases in the $Ni_{50}Mn_{34}In_{16}$ Heusler alloy. *Scr. Mater.* **2009**, *60*, 25–28.
6. Kainuma, R.; Imano, Y.; Ito, W.; Morito, H.; Sutou, Y.; Oikawa, K.; Fujita, A.; Ishida, K.; Okamoto, S.; Kitakami, O.; Kanomata, T. Metamagnetic shape memory effect in a Heusler-type $Ni_{43}Co_7Mn_{39}Sn_{11}$ polycrystalline alloy. *Appl. Phys. Lett.* **2006**, *88*, 192513.
7. Yu, S.Y.; Cao, Z.X.; Ma, L.; Liu, G.D.; Chen, J.L.; Wu, G.H.; Zhang, B.; Zhang, X.X. Realization of magnetic field-induced reversible martensitic transformation in NiCoMnGa alloys. *Appl. Phys. Lett.* **2007**, *91*, 102507.
8. Kainuma, R.; Ito, W.; Umetsu, R.Y.; Oikawa, K.; Ishida, K. Magnetic field-induced reverse transformation in B2-type NiCoMnAl shape memory alloys. *Appl. Phys. Lett.* **2008**, *93*, 091906.
9. Kim, Y.; Han, W.B.; Kim, H.S.; An, H.H.; Yoon, C.S. Phase transitions and magnetocaloric effect of $Ni_{1.7}Co_{0.3}Mn_{1+x}Al_{1-x}$ Heusler alloys. *J. Alloys Compd.* **2013**, *557*, 265–269.
10. Khovaylo, V.V.; Lyange, M.; Skokov, K.; Gutfleisch, O.; Chatterjee, R.; Xu, X.; Kainuma, R. Adiabatic temperature change in metamagnetic Ni(Co)-Mn-Al Heusler alloys. *Mater. Sci. Forum* **2013**, *738–739*, 446–450.
11. Rios, S.; Bufford, D.; Karaman, I.; Wang, H.; Zhang, X. Magnetic field induced phase transformation in polycrystalline NiCoMnAl thin films. *Appl. Phys. Lett.* **2013**, *103*, 132404.
12. Lyange, M.; Khovaylo, V.; Singh, R.; Srivastava, S.K.; Chatterjee, R.; Varga, L.K. Phase transitions and magnetic properties of Ni(Co)-Mn-Al melt-spun ribbons. *J. Alloys Compd.* **2014**, *586*, S218–S221.

13. Sharma, V.K.; Chattopadhyay, M.K.; Roy, S.B. Kinetic arrest of the first order austenite to martensite phase transition in $Ni_{50}Mn_{34}In_{16}$: dc magnetization studies. *Phys. Rev. B* **2007**, *76*, 140401.
14. Ito, W.; Ito, K.; Umetsu, R.Y.; Kainuma, R.; Koyama, K.; Watanabe, K.; Fujita, A.; Oikawa, K.; Ishida, K.; Kanomata, T. Kinetic arrest of martensitic transformation in the NiCoMnIn metamagnetic shape memory alloy. *Appl. Phys. Lett.* **2008**, *92*, 021908.
15. Xu, X.; Ito, W.; Tokunaga, M.; Umetsu, R.Y.; Kainuma, R.; Ishida, K. Kinetic arrest of martensitic transformation in NiCoMnAl metamagnetic shape memory alloys. *Mater. Trans.* **2010**, *51*, 1357–1360.
16. Xu, X.; Ito, W.; Tokunaga, M.; Kihara, T.; Oka, K.; Umetsu, R.Y.; Kanomata, T.; Kainuma, R. The thermal transformation arrest phenomenon in NiCoMnAl Heusler alloys. *Metals* **2013**, *3*, 298–311.
17. Nayak, A.K.; Suresh, K.G.; Nigam, A.K. Metastability of magneto-structural transition revealed by sweep rate dependence of magnetization in $Ni_{45}Co_5Mn_{38}Sb_{12}$ Heusler alloy. *J. Appl. Phys.* **2011**, *109*, 07A906.
18. Xu, X.; Ito, W.; Katakura, I.; Tokunaga, M.; Kainuma, R. In situ optical microscopic observation of NiCoMnIn metamagnetic shape memory alloy under pulsed high magnetic field. *Scr. Mater.* **2011**, *65*, 946–949.
19. Xu, X.; Kihara, T.; Tokunaga, M.; Matsuo, A.; Ito, W.; Umetsu, R.Y.; Kindo, K.; Kainuma, R. Magnetic field hysteresis under various sweeping rates for Ni-Co-Mn-In metamagnetic shape memory alloys. *Appl. Phys. Lett.* **2013**, *103*, 122406.
20. Kustov, S.; Corro, M.L.; Pons, J.; Cesari, E. Entropy change and effect of magnetic field on martensitic transformation in a metamagnetic Ni-Co-Mn-In shape memory alloy. *Appl. Phys. Lett.* **2009**, *94*, 191901.
21. Xu, X.; Ito, W.; Umetsu, R.Y.; Kainuma, R.; Ishida, K. Anomaly of critical stress in stress-induced transformation of NiCoMnIn metamagnetic shape memory alloy. *Appl. Phys. Lett.* **2009**, *95*, 181905.
22. Recarte, V.; Pérez-Landazábal, J.I.; Sánchez-Alarcos, V.; Zablotskii, V.; Cesari, E.; Kustov, S. Entropy change linked to the martensitic transformation in metamagnetic shape memory alloys. *Acta Mater.* **2012**, *60*, 3168–3175.
23. Niitsu, K.; Xu, X.; Umetsu, R.Y.; Kainuma, R. Stress-induced transformations at low temperatures in a $Ni_{45}Co_5Mn_{36}In_{14}$ metamagnetic shape memory alloy. *Appl. Phys. Lett.* **2013**, *103*, 242406.
24. Umetsu, R.Y.; Ito, K.; Ito, W.; Koyama, K.; Kanomata, T.; Ishida, K.; Kainuma, R. Kinetic arrest behavior in martensitic transformation of NiCoMnSn metamagnetic shape memory alloy. *J. Alloys Compd.* **2011**, *509*, 1389–1393.
25. Chernenko, V.A.; Cesari, E.; Kokorin, V.V.; Vitenko, I.N. The development of new ferromagnetic shape-memory alloys in Ni-Mn-Ga system. *Scr. Metall. Mater.* **1995**, *33*, 1239–1244.
26. Khovailo, V.V.; Oikawa, K.; Abe, T.; Takagi, T. Entropy change at the martensitic transformation in ferromagnetic shape memory alloys $Ni_{2+x}Mn_{1-x}Ga$. *J. Appl. Phys.* **2003**, *93*, 8483–8485.

27. Kainuma, R.; Gejima, F.; Sutou, Y.; Ohnuma, I.; Ishida, K. Ordering, martensitic and ferromagnetic transformations in Ni-Al-Mn Heusler shape memory alloys. *Mater. Trans.* **2000**, *41*, 943–949.
28. Okubo, A.; Xu, X.; Umetsu, R.Y.; Kanomata, T.; Ishida, K.; Kainuma, R. Magnetic properties of $Co_{50-x}Ni_xMn_{25}Al_{25}$ alloys with B2 structure. *J. Appl. Phys.* **2011**, *109*, 07B114.
29. Hasegawa, H.; Pettifor, D.G. Microscopic theory of the temperature-pressure phase-diagram of iron. *Phys. Rev. Lett.* **1983**, *50*, 130–133.
30. Ito, W.; Imano, Y.; Kainuma, R.; Sutou, Y.; Oikawa, K.; Ishida, K. Martensitic and magnetic transformation behaviors in Heusler-type NiMnln and NiCoMnln metamagnetic shape memory alloys. *Metall. Mater. Trans. A* **2007**, *38A*, 759–766.
31. L'vov, V.A.; Cesari, E.; Recarte, V.; Perez-Landazabal, J.I. Entropy change of martensitic transformation in ferromagnetic shape memory alloys. *Acta Mater.* **2013**, *61*, 1764–1772.
32. Uijttewaal, M.A.; Hickel, T.; Neugebauer, J.; Gruner, M.E.; Entel, P. Understanding the phase transitions of the Ni_2MnGa magnetic shape memory system from first principles. *Phys. Rev. Lett.* **2009**, *102*, 35702.
33. Entel, P.; Siewert, M.; Gruner, M.E.; Herper, H.C.; Comtesse, D.; Arroyave, R.; Singh, N.; Talapatra, A.; Sokolovskiy, V.V.; Buchelnikov, V.D.; Albertini, F.; Righi, L.; Chernenko, V.A. Complex magnetic ordering as a driving mechanism of multifunctional properties of Heusler alloys from first principles. *Eur. Phys. J. B* **2013**, *86*, 65.
34. Ito, W.; Nagasako, M.; Umetsu, R.Y.; Kainuma, R.; Kanomata, T.; Ishida, K. Atomic ordering and magnetic properties in the $Ni_{45}Co_5Mn_{36.7}In_{13.3}$ metamagnetic shape memory alloy. *Appl. Phys. Lett.* **2008**, *93*, 232503.
35. Segui, C.; Cesari, E. Composition and atomic order effects on the structural and magnetic transformations in ferromagnetic Ni-Co-Mn-Ga shape memory alloys. *J. Appl. Phys.* **2012**, *111*, 043914.
36. Xu, X.; Nagasako, M.; Ito, W.; Umetsu, R.Y.; Kanomata, T.; Kainuma, R. Magnetic properties and phase diagram of $Ni_{50}Mn_{50-x}Ga_x$ ferromagnetic shape memory alloys. *Acta Mater.* **2013**, *61*, 6712–6723.
37. Kainuma, R.; Oikawa, K.; Ito, W.; Sutou, Y.; Kanomata, T.; Ishida, K. Metamagnetic shape memory effect in NiMn-based Heusler-type alloys. *J. Mater. Chem.* **2008**, *18*, 1837–1842.
38. Ito, W.; Basaran, B.; Umetsu, R.Y.; Karaman, I.; Kainuma, R.; Ishida, K. Shape memory response in $Ni_{40}Co_{10}Mn_{33}Al_{17}$ polycrystalline alloy. *Mater. Trans.* **2010**, *51*, 525–528.
39. Kindo, K. 100 T magnet developed in Osaka. *Physica B* **2001**, *294*, 585–590.